Probing nanoscale structural and order/disorder phase transitions of supported Co-Pt clusters under annealing

Pascal Andreazza,[1,*] Christine Mottet,[2] Caroline Andreazza-Vignolle,[1] Jose Penuelas,[1,†] Helio C. N. Tolentino,[3] Maurizio De Santis,[3] Roberto Felici,[4] and Nathalie Bouet[1,‡]

[1]*Centre de Recherche sur la Matière Divisée, UMR 6619, Université d'Orléans-CNRS, 1 bis, rue de la Férollerie, 45071 Orléans Cedex 2, France*

[2]*Centre Interdisciplinaire de Nanosciences de Marseille, CNRS, Campus de Luminy, case 913, 13288 Marseille Cedex 9, France*

[3]*Institut Néel, CNRS and UFJ, 25 avenue des Martyrs, BP 166, 38042 Grenoble Cedex 9, France*

[4]*European Synchrotron Radiation Facility, BP 220, 38048 Grenoble Cedex 9, France*

Structural and order/disorder phase transitions in bimetallic $Co_{50}Pt_{50}$ nanoparticles induced by annealing have been investigated combining *in situ* small and wide angle x-ray scattering methods. The support of Monte Carlo simulations within a semiempirical tight-binding potential provides a realistic description of the CoPt cluster structure in the size (1.5–3.5 nm) and temperature (300–900 K) ranges, in good correlation with the experiments. If a coalescence process of as-grown noncrystalline icosahedral clusters (2 nm) induced by annealing is detected at low temperature (<600 K), higher temperatures (>700 K) are necessary to induce, by internal atom rearrangement, the formation of decahedral structure followed by a transition to an fcc structure. We demonstrate that the expected chemical ordering occurs only from particles of fcc structure. The investigation of the chemical order/disorder transition of 3.5 nm-sized nanoparticles reveals a bistability state around 900 K with a bimodal distribution corresponding to a coexistence of almost fully ordered nanocrystals and fully disordered ones, also supported by theoretical calculations, suggesting a first-order transition in clusters as in bulk alloys.

I. INTRODUCTION

Bimetallic nanoparticles (NPs) have received considerable attention because, besides the size reduction effect, the addition of a second metal provides a method to control their properties and functionalities.[1,2] In the field of magnetic recording, most efforts have been concentrated on the increase in magnetic storage density and consequently, size reduction in magnetic building blocks, such as NPs.[3] A promising way is to design alloy clusters consisting of a combination of a $3d$ metal with a high-spin moment (Fe, Co) and $4d$ or $5d$ metals (such as Pd, Rh, or Pt) which induces a large orbital magnetic moment (via the strong spin-orbit coupling). As a consequence the magnetic anisotropy is enhanced[4] and the cluster magnetization stabilized against thermal fluctuation. According to the bulk phase diagram,[5] at the equiatomic composition, a face centered tetragonal $L1_0$ ordered phase can be obtained at low temperature, below the order/disorder transition temperature while the face centered cubic (fcc) A1 chemically disordered phase is thermodynamically stable above. In the case of nanoparticles, theoretical studies predicted that this critical temperature should decrease with the particles size.[6–8] However, experimental observations of the $L1_0/A1$ transition are difficult because as-synthesized FePt or CoPt particles exhibit a chemically disordered structure. Thus a postsynthesis annealing is necessary to provide the needed atom mobility to transform the disordered phase to the ordered equilibrium $L1_0$ one, keeping the temperature below the order/disorder transition temperature of the considered clusters size. Consequently, most of the experimental studies concentrate their efforts to optimize the synthesis methods and the annealing processes in such a way that the

nanoparticles can order at relatively low temperature, without increasing their size by coalescence or Ostwald ripening mechanism.[9,10] However, the main limitation to this optimization is the possibility to investigate *in situ* each step of the annealing process to elucidate the mechanism of morphological and phase transitions at these sizes. The most convincing experimental studies are performed *ex situ* postannealing using high-resolution transmission electron microscopy (TEM) where the NPs are embedded in a matrix[11] or epitaxially grown on an MgO(100) surface[12] or on an amorphous carbon film[13] and sometimes covered by a thin amorphous alumina film.[14] Because of the influence of different capping layers on the NPs facets or the kinetic history of the nanoparticles growth method, the as-grown chemical and structural characteristics of these NPs shows a substantial difference with respect to their equilibrium counterparts.[8,15] In addition, these works exhibit divergent and sometimes, conflicting results mainly due to the influence of different preparation conditions. Here we propose an *in situ* x-ray scattering investigation on weakly interacting bare CoPt NPs in ultrahigh vacuum (UHV) in order to get a quantitative description of the temperature and size effects on their structure by minimizing the effect of their environment.

For most transition-metal free-capping NPs, experimental observations revealed frequently a noncrystalline multitwinned morphology [decahedron (Dh) fivefold twin or icosahedron (Ih) twin] at small sizes[13,16,17] because the surface energy gain in forming only (111) facets supersedes the cost of twin interfaces and internal strains[18] in equilibrium conditions. However, *in situ* analyses of CoPt NPs grown at room temperature (RT) by vapor deposition reveal the icosahedral

structure up to 3 nm in size[19] whereas similar *ex situ* studies at equivalent size[11,13] reveal mainly a fcc structure (truncated polyhedra). In this case, environment effects or kinetic factors over the growth can extend the size range where such structures are observed even if they are no more thermodynamically stable. Furthermore, our previous results[19] showed the possible change from Ih to Dh structure by direct annealing at 770 K. We propose in this study to elucidate the role of the NPs initial structure on the disorder/order transition, knowing that the NPs noncrystallinity (Ih or Dh) is a limiting factor to achieve a high degree of chemical order.[8] Our aim is to understand what are the necessary steps to achieve the $L1_0$ nanosized phase from an Ih structure during annealing. For this reason, *in situ* characterizations of CoPt clusters evolution by synchrotron radiation scattering measurements were performed step by step from the as-grown room temperature to the ordering temperature. In addition, the support of Monte Carlo simulations within a semiempirical tight-binding (TB) potential provided an unambiguous identification of the CoPt NPs structure and a strengthening of observed transition mechanisms. We show how to take advantage of the coalescence mechanisms to tune the nanoparticles crystallinity and to yield ordered structures, and reveal a thermodynamically bistability state of nanoparticles in the order/disorder transition temperature range.

The paper is composed of six sections including the introduction and the conclusion. The Sec. II is devoted to the experimental methods, the Sec. III to the experimental results, the Sec. IV to the theoretical insights and the Sec. V to the discussion.

II. EXPERIMENTAL METHODS

The equiatomic CoPt NPs are prepared *in situ* at RT by vapor deposition on thermally oxidized Si(100) wafers covered by an amorphous carbon layer in ultraclean environment.[13] Nanoparticles surface can be considered as free, apart the interface with the substrate. The composition of the nanoparticles assembly is measured by an average method, the Rutherford backscattering and a local method, the energy dispersive x-ray spectroscopy, in order to check the equiatomic balance (+−5%) between Co and Pt atoms. This composition influences the degree of order which can be achieved in the NPs and must be also a critical parameter for the stability of different morphologies.[20,21] After RT preparation, the samples are *in situ* heated by electron beam furnace in order to reach quickly (in 5 mn) the nominal requested temperature which is stabilized at least during 1 h. The sample temperature is calibrated by a thermocouple situated at the back of the sample and double checked with an infrared pyrometer.[19]

Because the determination of the atomic structure at the nanoscale is a complex problem, methods that can probe local and average nanoparticles features as well as nanometer-to micrometer-lengh scale, provide highly complementary informations about their structure and morphology and are much powerful when used together.[22–24] *In situ* grazing incidence small-angle x-ray scattering (GISAXS) and grazing incidence x-ray diffraction (GIXD)
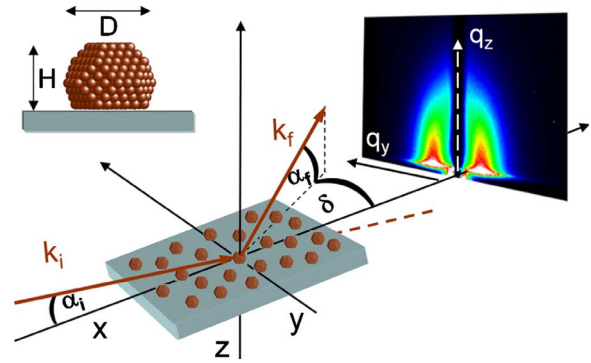
FIG. 1. (Color online) X-ray scattering measurements geometry. The sample is irradiated by a monochromatic x-ray beam of 20 keV at a fixed grazing incidence α_i of 0.07 and the scattered intensity is as a function of the out-of-plane angle α_f with respect to the substrate surface and of the in-plane angle δ. The components of the wave-vector transfer $q = k_i − k_f$, defined by the incident k_i and the scattered k_f wave vectors are $q_x = |k_i|(\cos \alpha_f \cos \delta − \cos \alpha_i)$, $q_y = |k_i|(\cos \alpha_f \sin \delta)$ and $q_z = |k_i|(\sin \alpha_f + \sin \alpha_i)$ in the laboratory frame (Refs. 24 and 27). Experimentally, the GISAXS intensity is recorded on a two-dimensional detector, perpendicular to the *x* axis, as a function of the in-plane q_y and out-of-plane q_z components. The GIXD intensity is recorded on a zero-dimensional detector as a function of the in-plane angle δ whereas the out-of-plane α_f angle is fixed to the α_i value.

have been used simultaneously, during the annealing experiments (from 300 to 900 K), allowing the determination of the structure at the atomic scale range (small angles) and at the particle scale range (wide angles), respectively. To confirm the results, these investigations have been performed on two different beamlines at ESRF (European Synchrotron Radiation Facility, Grenoble, France), ID03 and the french CRG BM32 beamlines using an UHV setup to avoid any post-deposition contamination.[25,26] Due to the low quantities of deposited metal, the x-ray grazing incidence angle has been selected in order to reduce the scattering background from amorphous substrate and simultaneously to maximize the scattering contribution of metals. Combined simultaneous GISAXS and GIXD patterns are recorded in a standard framework used in grazing incidence geometry, detailed in Fig. 1. The morphological analysis procedure is based on the adjustment between the two-dimensional GISAXS patterns with simulated scattering spectra obtained from a dedicated code.[28] The quantitative structural analysis is performed in the similar way, facilitated by Monte Carlo simulations of CoPt nanoalloys using a semiempirical tight-binding potential.[8] To validate the scattering results, *ex situ* TEM measurements have been performed post *in situ* annealing and also before annealing on equivalent samples.

III. *IN SITU* EXPERIMENTS

The as-grown particles exhibit a monodisperse size distribution ($D = 1.9 \pm 0.5$ nm) as displayed in the TEM micrograph in Fig. 2(a). These results are in agreement with *in situ* GISAXS measurements [Fig. 2(b)] used to quantify the NPs diameter *D* and height *H*, and the correlation distance Λ, i.e.,
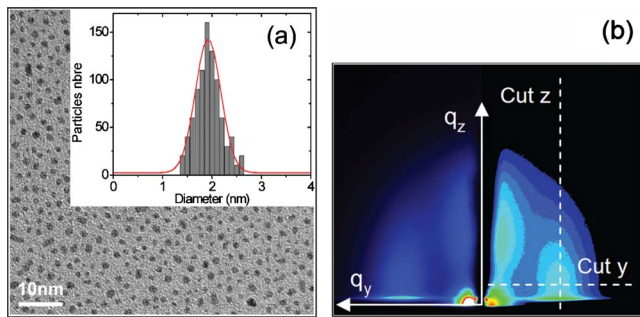
FIG. 2. (Color online) (a) TEM micrograph and size distribution histogram of as-grown CoPt NPs prepared at 300 K. (b) *in situ* measured GISAXS pattern of the same sample, corresponding to 5×10^{15} atoms/cm^2. The two cuts of the intensity, i.e., cross sections, in the q_y and q_z directions, selected in the lobe intensity region (dash lines) are simultaneously fitted with the IsGisaxs code (Ref. 28).

center to center distance between particles (the details of the analysis procedure[29] are described elsewhere). The morphological results give $D = 1.9$ nm and $H = 1.3$ nm, with a relative geometrical standard deviation $\sigma(D)/D = 0.3$. In addition, the experimental diffraction (GIXD) pattern was compared to calculated spectra for several parameterized structural models [truncated octahedra (TOh) based on fcc structure, Dh and Ih], based on the Debye equation.[29–31] As shown in our previous study,[19] the structure of RT as-grown CoPt nanoparticles is in agreement with the icosahedral chemically disordered model. Core-shell models were also considered with a shell thickness of one monolayer as mentioned in the literature,[15] and corresponding calculated spectra exhibit no difference with respect to fully mixed models in this size range. In addition, due to the weak metal-cluster/carbon-substrate interactions, the NPs are randomly oriented on the substrate without significant preferential crystallographic orientation.

Then, the sample has been heated step by step ($\Delta T = 30° - 50°$) from 300 to 900 K in UHV conditions (10^{-10} mbar range) during the x-ray scattering data collection. Figure 3 shows a selected GIXD patterns set corresponding to different ranges of annealing temperatures. Up to 600 K, the diffraction patterns agrees with the Ih chemically disordered structure without size modification [Fig. 3(a)]. At higher temperatures (700 to 800 K), the NPs fit well with noncrystalline Dh model (with sizes around 3 nm). Then, at 820 K [Fig. 3(c)], the best fit is obtained by mixing Dh and TOh-fcc chemically disordered models (around 50% each in atomic fraction) of around 3.5 nm in diameter, i.e., around $N = 2000$ atoms.

GISAXS patterns have been also recorded during the annealing. Figure 4 reveals the evolution versus substrate temperature of the NPs morphology through that one of three characteristic lengths: the average interparticle distance Λ, diameter D and height H, that was deduced from intensity cross-sections evolutions. From the correlations between H and D and between Λ and D, in Figs. 4(a) and 4(b), respectively, two stages can be distinguished in these evolutions with a behavior change at 600–700 K. Below this temperature, the height is nearly constant while the diameter in-
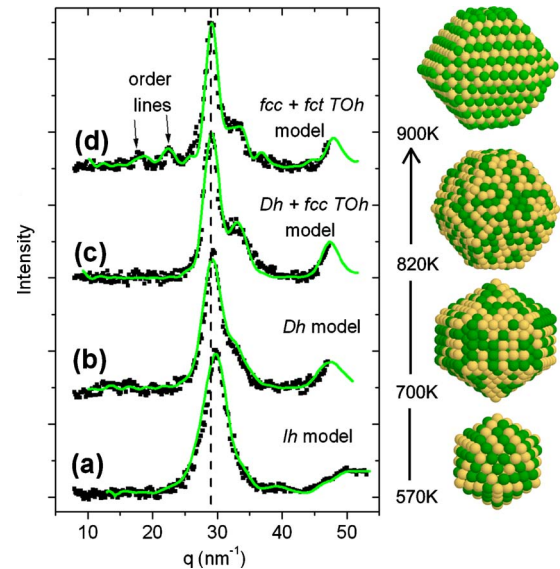
FIG. 3. (Color online) Selected experimental and calculated GIXD spectra using Monte Carlo relaxed CoPt clusters at increasing annealing temperature: (a) 570 K with icosahedral (Ih) fit models (b) 700 with decahedral (Dh) fit models (c) 820 K with Dh and TOh mixture fit models and (d) 900 K with TOh fit models. The insets show the snapshots of different simulated clusters (Co and Pt atoms are represented as light and dark spheres, respectively). A vertical dashed line corresponding to the fcc (111) line is given for comparison.

creases. Above 700 K, the particles get rounded as H/D evolves from 0.7 to 0.95. At the same time, the correlation distance Λ value jumps from 4 to 6 nm [Fig. 4(b)] and remains quasi constant until 900 K while the spacing disorder parameter $\sigma(\Lambda)/\Lambda$, i.e., the standard deviation of the NPs distance correlation function,[24] increases from 0.3 to 0.5.

Below 820 K, the diffraction patterns are in agreement with chemically disordered structures with an interatomic distance of 0.266 nm, close to the A1 Co$_{50}$Pt$_{50}$ bulk value of 0.265 nm. Above this temperature, additional superlattice peaks corresponding to alternate pure Co and pure Pt planes in the close-packed CoPt structure, are detected [Fig. 3(d)]. These peaks are the signature that the chemical ordering mechanism leading to the tetragonal L1$_0$ NPs formation becomes effective around 900 K. At this temperature, the size and shape of NPs remain nearly unchanged [Fig. 4(b)] with respect to those at 820 K. Thus, the ordering develops by atomic rearrangement at constant particle size. The degree of order can be evaluated thanks to an analysis of the diffraction pattern. Commonly, the long-range order parameter[32] (LRO) is obtain from the ratio of superlattice-to-fundamental (001)/(002) peak intensities in the L1$_0$ structure, taking into account atomic scattering factors and correction factors (setup geometry, Debye-Waller).[33,34] A more convenient method is to extract the radial distribution function from the wide-angle scattering pattern[35,36] but the overlapping between large peaks due to the small size of particles and the short angle range of data may induce an uncertainty on the structure identification. It seems to us, the more accurate method is to fit experimental data with simulated patterns of Monte Carlo calculated ordered clusters corresponding to different LRO
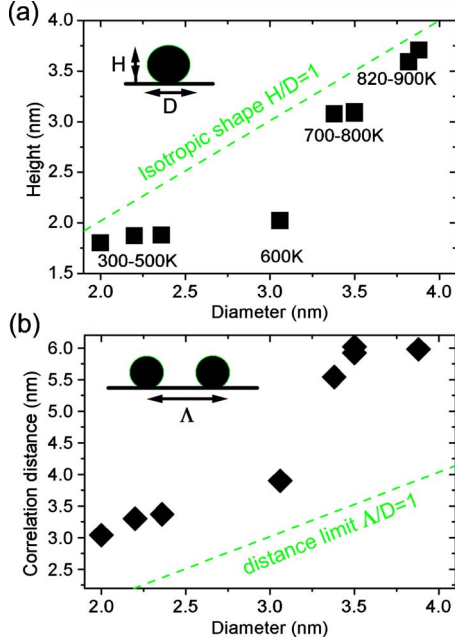
FIG. 4. (Color online) Evolution of morphological parameters during annealing: correlation between (a) the height H or (b) the distance between particles Λ and the diameter D during the temperature increase (parameters extracted from GISAXS experimental pattern, i.e., q_z and q_y cross sections). The dashed lines correspond to (a) an isotropic shape, i.e., an aspect ratio of 1 and (b) the limit of minimum spacing between particles, i.e., a maximum coverage of the substrate surface.

parameters (Fig. 5). This gives us, at the same time, the chemical order and structural nature of the annealed NPs.

IV. THEORETICAL INSIGHTS

The theoretical investigation of the structure, morphology, and chemical ordering of CoPt NPs is performed by canonical Monte Carlo simulations, within the standard Metropolis algorithm, using a semiempirical many-body potential. We chose the TB second moment approximation (TB-SMA) potential as described by Rosato, Guillopé, Legrand[37] on pure transition and noble metals and extended to their alloys by
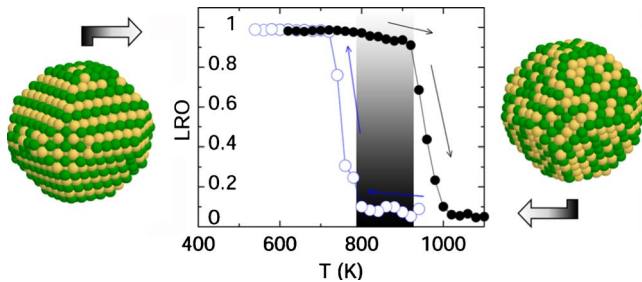
FIG. 5. (Color online) Plot of long-range order (LRO) parameter of the 1289 atoms TOh and snapshots of quite fully ordered and fully disordered clusters in the 900 K temperature range. The order-disorder transition occurs around 950 K in the annealing process (black points) and around 750 K in the cooling process (open blue circles).

Cleri and Rosato.[38] In this approximation, the energy is writing in a simple analytical form with one attractive term coming from the band structure in tight-binding theory where the density of state is approximated by its second moment (band width):

$$E_{n,i}^b(\{p_m^j\}) = - \sqrt{\sum_{\substack{m \\ r_{nm} < r_c}} \sum_{j=A,B} p_m^j \xi_{ij}^2 e^{-2q_{ij}(r_{nm}/r_{ij}^o - 1)}} \quad (1)$$

and is counterbalanced by a repulsive term of the Born-Mayer type,

$$E_{n,i}^r(\{p_m^j\}) = \sum_{\substack{m \\ r_{nm} < r_c}} \sum_{j=A,B} p_m^j A_{ij} e^{-p_{ij}(r_{nm}/r_{ij}^o - 1)}, \quad (2)$$

where r_{nm} is the distance between the atoms at sites n and m, $r_{ii}^o, i=A,B$, is the first-neighbor distance in the pure metal i, $r_{ij}^o = (r_{ii}^o + r_{jj}^o)/2$ if $i \neq j$, and r_c is the cut-off distance for the interactions between the second and third neighbors. $\{p_m^j\}$ represents the chemical configuration of the system, in which p_m^j is the occupation number equal to 1 or 0 depending on that the site m is occupied or not by an atom of chemical type $j, (j=A,B)$ (for a binary alloy AB, $p_m^A = 1 - p_m^B = p_m$). The parameters $(A_{ij}, p_{ij}, q_{ij}, \xi_{ij})$ are fitted to different experimental values and have been taken from the reference.[8]

The total energy of the system is then written as follows:

$$E_{tot}[(p_n^i)] = \sum_n \sum_{i=A,B} p_n^i \{E_n^{i,b}[(p_m^j)] + E_n^{i,r}[(p_m^j)]\}. \quad (3)$$

Such potential is equivalent to the embedded atom method developed by Daw and Baskes[39] and extended to the metallic alloys by Foiles.[40] We must keep in mind the limitations of such energetical approach fitted on bulk properties. They may be not transferable to surfaces or nanoparticles as far as the surfaces and clusters display low-coordinated sites. In particular, such potentials are known to underestimate the surface energy but keeping most of the time a quantitative good energy difference between the metals. This is the case for the Co-Pt system where despite an underestimation of the surface energy of each pure metal (see Table I), their difference is reasonable as compared to experimental or *ab initio* value, which is a good point in the description of the surface segregation. As the difference in the surface energy is weak (so that even the sign does not matter!), the surface segregation will not be very strong as it is the case in the Cu-Ag system $\Delta\gamma_{Ag-Cu}^{(100)} = 0.55$ (J/m²), for example, for which well-defined core/shell structures are obtained.[44–46] The second important driving force for surface segregation is the chemical ordering or demixion tendency (which depends on the bulk alloy phase diagram). The demixion tendency favors the core/shell structure by a phase separation process (which is the case of Cu-Ag) whereas an ordering tendency leads to an oscillating profile near the surface with the segregation of the majoritary species. As we consider here nanoalloys at equiconcentration, this effect will not have a strong influence on the segregation. We checked that after the fit to the solution energies of a Co impurity in the Pt bulk and of a Pt impurity in the Co bulk, the formation energies of the main

TABLE I. Surface energy of pure Co and pure Pt and of Co or Pt terminated $L1_0$. Formation energies of the A1, $L1_0$ and $L1_2$ phases of the Co-Pt system. c/a ratio in the tetragonal $L1_0$ phase. (a) Ref. 41, (b) Ref. 42, and (c) Ref. 43, calculated with the same method used in Ref. 41.

	TB-SMA	DFT[a]	Expt.
$\gamma_{Co}^{(100)}$ (J/m^2)	1.165	2.110[a]	2.55[b]
$\gamma_{Pt}^{(100)}$ (J/m^2)	1.282	1.840[a]	2.48[b]
$\Delta\gamma_{Pt\text{-}Co}^{(100)}$ (J/m^2)	0.117	−0.270[a]	−0.07[b]
Co terminated $(100)L1_0$ (J/m^2)	1.63		
Pt terminated $(100)L1_0$ (J/m^2)	0.96		
ΔE^{A1} (eV/at.)	−5.26		−5.16[c]
ΔE^{L1_0} (eV/at.)	−5.35	−5.374[c]	−5.33[c]
ΔE^{L1_2} (eV/at.)	−5.62		−5.63[c]
c/a	0.93	0.98[c]	0.97[c]

[a]Reference 41.
[b]Reference 42.
[c]Reference 43.

ordered phases [$L1_0$ and $L1_2$ (Ref. 5)] have the right value as compared to the bulk phase diagram (see Table I). The potential underestimates the bulk critical temperature transition from the $L1_0$ ordered phase to the A1 disordered phase by about 200 K and overestimates the tetragonalisation (see Table I). The shift in temperature has to be taken into account when comparing to the experimental temperatures. However, this semiempirical model succeeded to give a quantitative decrease in the critical temperature of order disorder with cluster size.[14] Finally, the third important driving force to the surface segregation is the lattice misfit which makes segregate the larger element. Our potential leads to the surface terminaison by Pt in the $L1_0$ phase in good agreement with the density-functional theory (DFT) calculations[15,41,47] (see Table I).

The *ab initio* DFT calculations are of course much accurate because not parametrized but still much time consuming. For exemple, they have been used for relatively small nanoalloys[47] (less than 100 atoms) or for more extended systems[15] (about 600 atoms) but on a much more restricted number of explored configurations whereas Monte Carlo simulations coupled to a semiempirical potential cover a much larger spectrum of structures in the configurations space. So we still have to choose between a full statistic sampling of the configurations space or an accurate calculation from the point of view of the electronic structure.

We first concentrate on the structural transition from noncrystalline to crystalline structures at 0 K and at finite temperature. Pure Pt and pure Co clusters undergo structural transition at 0 K as a function of the cluster size from Ih to fcc TOh going through the Dh structure.[18] For Pt, Dh clusters are stable between 75 (1 nm) and 5000 atoms (4.5 nm). For Co clusters, the transitions are shifted to higher sizes, respectively, to 2 nm and 5–6 nm. The question still remains concerning structural transition in CoPt clusters. A DFT study[15] showed that ordered core/shell Ih and Dh are more favorable than the $L1_0$ phase ordered fcc clusters up to 2.5 nm in size, i.e., about 600 atoms. However, this study compared essen-
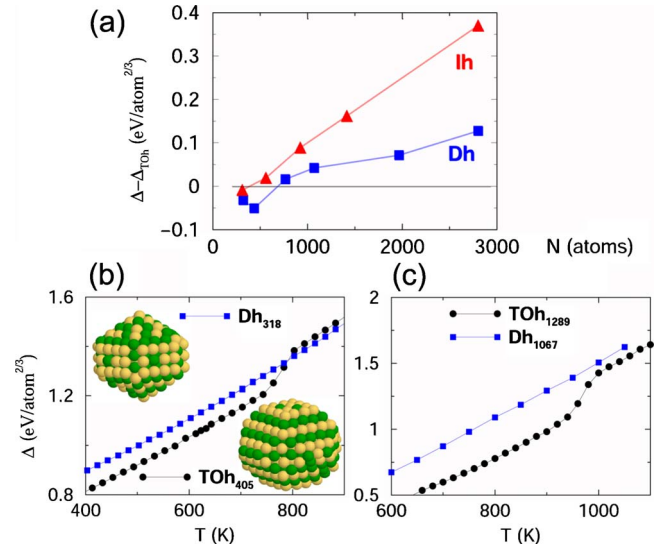
FIG. 6. (Color online) (a) Normalized excess energy (at 0 K) of the different cluster models for icosahedra (Ih: 309, 561, 923, 1415, and 2057 atoms, red triangles) and decahedra (Dh: 318, 434, 766, 1067, 1965, and 2802 atoms, blue squares) relatively to the one of truncated octahedra (TOh: 201, 314, 405, 807, 1289, 2075, and 2951 atoms, zero line) versus the cluster size at equiconcentration. In graphs (b) and (c) the same quantity Δ versus temperature is plotted for the 405 atoms TOh (black points) and the 318 Dh (blue squares) in graph (b) and for the 1289 atoms TOh (black points) and the 1067 atoms Dh (blue squares) in graph (c).

tially the fivefold symmetry structures (Ih, Dh) to the cuboctahedron fcc morphology which is not the best optimized fcc morphology. To minimize the surface energy and thus optimize the fcc structure, the (100) facets have to be reduced to the benefit of the (111) facets with lower energy. This leads to the truncated TOh with a different number of atoms than the Ih. Even the Dh can be optimize to give the Mackay decahedron[18] giving one more time a different number of atoms. To overcome the difficulty to compare structures with different atoms numbers, we use the normalized excess energy given by

$$\Delta = (E_{cluster} - N_{Co}E_{Co}^{coh} - N_{Pt}E_{Pt}^{coh})/N^{2/3}, \qquad (4)$$

where N_i and E_i^{coh} are the number and cohesion energy of the metal i.

To optimize the structures at 0 K, quenched molecular dynamics are performed after the Monte Carlo simulations. The Fig. 6(a) displays the relative energy of Ih and Dh as referred to the TOh one at 0 K. We see clearly that the $L1_0$ orderedlike Dh is the more stable structure starting from about 300 atoms up to about 700 atoms, then the ordered $L1_0$ TOh becomes the more stable one. At smaller sizes (less than 100 atoms), *ab initio* DFT calculations[47] confirmed the polyicosahedral structures obtained by global optimization using the same potential as the one used here.[8]

At finite temperature, NPs undergo an order-disorder transition (see Fig. 5) with a hysteresis which is a signature of a first order transition as in the bulk alloy. This ordering could

affect the relative energy of Dh and TOh structures when comparing theoretical and experimental results. The Figs. 6(b) and 6(c) show two selected examples of the internal energy evolution with the temperature of Dh and TOh clusters of around 2 nm (c) and around 3 nm (d). Although both the structures undergo an order/disorder transition from low temperature to high temperature, only the TOh clusters display a jump in the internal energy with a transition from the $L1_0$ type ordering to the A1 disordered state. This transition in the internal energy is not necessary in a typical chemical transition since only the entropy in the free-energy expression is generally concerned.[48] However, we wanted to point out here that in nanoalloys, when many structures coexist with very weak-energy differences, such internal energy variation could affect the temperature phase diagram. In our case, the stability of the 1289 atoms TOh at low temperature is almost equivalent to the 1067 atoms Dh at high temperature (1000 K) because of the disordering of the TOh $L1_0$ cluster. In the case of the 2 nm size clusters, there is even an inversion in the stability of the 405 TOh cluster to the benefit of the 318 Dh one at 800 K.

V. DISCUSSION

Our results for CoPt NPs reveal several structural transitions (from Ih to TOh models) during annealing, yielding chemically disordered clusters at low temperature, followed by an ordering at higher temperature and larger size. At RT, the isolated particles are in an icosahedral structure, which is a metastable state according to the theoretical calculation of stable structures at 0 K, and can be interpreted by a kinetic trapping during their atom-by-atom growth. At low temperature (400 K), the annealing induces a weak coarsening due to an Ostwald ripening to the benefit of larger NPs with respect to the ultra small NPs ($D < 1$ nm), without any change in the structure.

Around 600 K, an aggregation mechanism occurs with the diffusion of the less trapped particles that stick to others leading to aggregated particles. This is illustrated on Fig. 4 where Λ and D increase while H remains almost constant. At the same time, the wide angle GIXD patterns indicate that the structure of individual particles forming the aggregate remains Ih with an unchanged size distribution. This indicates that the mechanism results only in a motion-sticking of clusters without atoms rearrangement among particles.

At 700 K, a complete coalescence process occurs: neighboring particles merge into a larger one occupying the mass center of two previous ones. The shape of the particles is tridimensionally modified ($H \sim D$), yielding to another multitwinned structure: the decahedron. The Ih-Dh transition temperature is moderated, which suggests that this transition is rather induced by the coalescence process. Ding *et al.*[49] have shown that the coalescence temperature, i.e., the temperature corresponding to a complete coalescence from two particles into a single one, decreases for smaller particles because their larger surface curvature facilitates surface diffusion. On the other hand, several groups[50,51] found that misaligned nanoparticles rotate to form low energy interfaces during sintering. In our case, the weak interactive amorphous

carbon substrate and the motion of the NPs on the substrate by thermal activation are in favor of the formation of such multitwinned particles. In addition, our theoretical calculations show that the chemical disorder favors the stability of multitwinned particles at higher size than expected as compared to disordered TOh NPs [Figs. 6(b) and 6(c)]. These combined mechanisms could explain the formation of Dh structure in the 3 nm-size range.

At higher temperature (around 800 K), a structural transition from Dh to fcc TOh clusters is observed as predicted by the phase diagram as a function of NPs size. At the same time, the NPs size increases and their shape becomes more and more isotropic, similarly to the ones obtained without support effect. The mechanism is similar to a particle ripening leading to the most stable structure at larger NPs size close to the equilibrium conditions in agreement with the calculations giving the TOh more stable from 3 nm and above. Although the thermal activation is sufficient to induce the atomic rearrangements leading to the stable atomic structure at this size, the NPs are still chemically disordered [see Fig. 4(c)].

Finally, the chemical ordering is obtained at 900 K (Fig. 3) at fixed cluster size. These structural evolution from non-crystalline to $L1_0$ crystalline structure reveals a strong dependence between the CoPt nanoparticle structure and their ordering. Indeed, the expected chemical ordering occurred only from crystalline disordered structure. The noncrystallinity of nanoparticles (Ih or Dh) is a limiting factor to achieve the chemical order. In a first step, the combined effect of the diffusivity enhancement and the coalescence mechanism due to the annealing favor the transition of as-grown icosahedral particles toward the fcc structure. In a second step, the disorder-order transition can occur by temperature-induced internal diffusion from the lower energy nanoparticle structure, the fcc TOh structure.

To evaluate the degree of order of annealed particles, selected CoPt TOh clusters (Fig. 5) have been simulated in the temperature range of the theoretical transition (800–1000 K corrected temperatures). The Fig. 7(a) displays the wide-angle scattering profiles of the four different calculated clusters of same size (1289 atoms, 3 nm) corresponding to different LRO. The extinction of the peaks (001) and (110) corresponding to the high symmetry fcc structure and the splitting of (200)/(002) and (220)/(202) peaks due to the tetragonalization ($a \neq c$) are clearly distinguishable in the pattern of the ordered clusters. Figure 7(b) shows the comparison between the experimental pattern obtained at 900 K and simulated patterns from a partial order cluster (LRO=0.44) and a mix of ordered-disordered clusters. In both cases, the main requirement of the fitting was the intensities scaling adjustment of the superlattice peaks (110)-(001) and the main peak (111) with the experimental pattern. An excellent matching is obtained with a mixture of 65% (in atoms) of ordered clusters and 35% of disordered clusters. These results show that a bimodal distribution of fully chemically ordered NPs and fully disordered ones is more realistic than a distribution of partially ordered ones.

This result is a nice overview of the nature of the transition since up to now, experimental results performed by transmission electron microscopy did never give such statis-
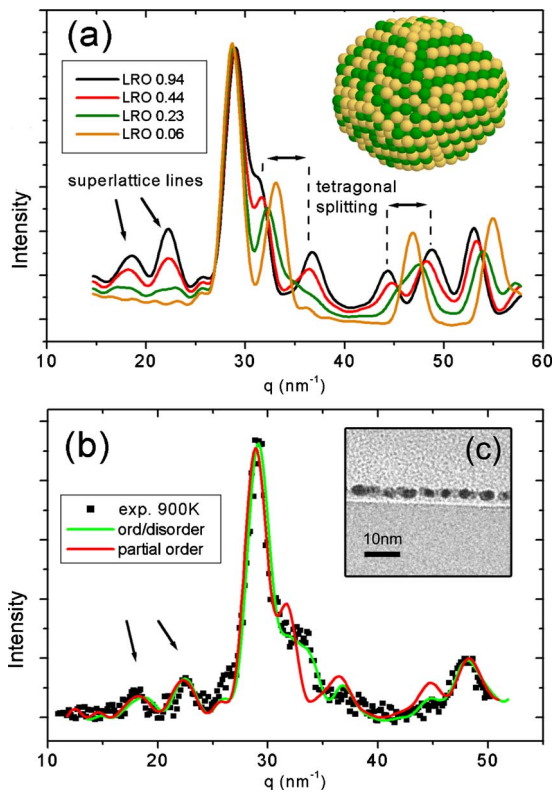
FIG. 7. (Color online) Calculated GIXD spectra of (a) four different MC relaxed truncated octahedron CoPt clusters of same size (1289 atoms) corresponding to LRO of 0.06, 0.23, 0.44, and 0.94 according to the Cowley definition (Ref. 32); (b) Comparison between 900 K-annealed NPs experimental(square marks) and calculated (solid line) diffraction patterns. The simulated patterns correspond to a partial ordered cluster (LRO=0.44) as illustrated in the insert, and a mix of ordered-disordered clusters, in green and red color, respectively. (c) TEM micrograph of a cross section of the sample quenched from 900 K.

tical average on the ordering state of a complete distribution of nanoparticles. In a perfect agreement with the theoretical results where the hysteresis on the order-disorder transition between the heating curve and the cooling curve (Fig. 5) plays in favor of a coexistence of the two states in a certain temperature range (800–1000 K), the x-ray diffraction results are better fitted by a bimodal distribution of ordered and disordered NPs than by an homogeneous distribution of partially ordered NPs. It is important to notice that the model structures obtained by the Monte Carlo simulations do not give an homogeneous partially ordered structure for LRO=0.44 which would be in contradiction with the bistability of the ordered and disordered state. It is rather a transition state with the coexistence of an ordered part and the nucleation of a disordered part inside the same particle [see the insert of Fig. 7(a)]. We checked over a simulation at constant temperature (in the coexistence range) that the transition from one state to the other can take place but such transition remains very rare in our simulation time (100 millions Monte Carlo steps). A similar bistability has been re-

cently evidenced theoretically on the segregation transition of CuAg clusters,[44] without experimental comparison.

VI. CONCLUSION

We have provided a quantitative description of the structural and chemical order-disorder phase transitions of 1.5 to 4 nm bimetallic $Co_{50}Pt_{50}$ nanoparticles induced by increasing annealing temperatures (300–900 K). The combined morphological and structural analysis at nanometer scale is given by an *in-situ* x-ray scattering method at wide and small angles together with the support of Monte Carlo simulations within a semi-empirical tight-binding potential providing a realistic description of the CoPt nanoparticles structure (crystalline or noncrystalline, order degree). If a coalescence process of as-grown icosahedral particles (2 nm) induced by annealing is detected at low temperature (<600 K), higher temperatures (>700 K) are necessary to the formation of decahedral structure by atomic rearrangement, followed by a transition to the fcc morphology and finally, a chemical ordering around 900 K at fixed particle size. No direct structural transition from non-crystalline to $L1_0$ structure seems possible. Indeed, the chemical ordering occurred only from fcc disordered nanoparticles. In addition, contrary to what has been suggested in the literature, the investigation of the order/disorder transition at fixed size reveals a bistable state of the nanoparticles at 900 K with a bimodal distribution population corresponding to a coexistence of almost fully chemically ordered and fully disordered particles, as expected by theoretical calculations, suggesting a first-order transition in clusters.

A still remaining question is the competition between the out-of-equilibrium growth conditions and the equilibrium state. The heating is performed on growing NPs and the dynamical coalescence process, which results in the structural transition from Ih to Dh and, then, in the transition toward the equilibrium atomic fcc structure, has been clearly identified. After such a growth process, the phase is still chemically disordered. The heating procedure is used to activate the internal diffusion in order to get the chemically ordered $L1_0$ tetragonal structure. Such structure is well characterized experimentally at 900 K. This is in agreement with the theoretical phase diagram which suggests that NPs of 3 nm and above should be ordered.[14] However, it would be worth to check, starting with an ordered NPs distribution, if the NPs becomes disordered by increasing the annealing temperature or ordered by cooling down. Such investigation is still in progress.

*Corresponding author; pascal.andreazza@univ-orleans.fr

†Present address: INL, Ecole Centrale de Lyon, Ecully, France.

‡Present address: NSLSII, Brookhaven National Laboratory, P.O. Box 5000, NY 11973-5000, United States.

[1] B. Corain, G. Schmid, and N. Toshima, *Metal Nanoclusters in Catalysis and Materials Science: The Issue of Size Control* (Elsevier, Amsterdam, The Netherlands, 2007).

[2] R. Ferrando, J. Jellinek, and R. L. Johnston, Chem. Rev. **108**, 845 (2008).

[3] P. Gambardella, S. Rusponi, M. Veronese, S. S. Dhesi, C. Grazioli, A. Dallmeyer, I. Cabria, R. Zeller, P. H. Dederichs, K. Kern, C. Carbone, and H. Brune, Science **300**, 1130 (2003).

[4] P. Bruno, Phys. Rev. B **39**, 865 (1989).

[5] C. Leroux, A. Loiseau, D. Broddin, and G. Vantendeloo, Philos. Mag. B **64**, 57 (1991).

[6] R. V. Chepulskii and W. H. Butler, Phys. Rev. B **72**, 134205 (2005).

[7] B. Yang, M. Asta, O. N. Mryasov, T. J. Klemmer, and R. W. Chantrell, Acta Mater. **54**, 4201 (2006).

[8] G. Rossi, R. Ferrando, and C. Mottet, Faraday Discuss. **138**, 193 (2008).

[9] Z. R. Dai, S. Sun, and Z. L. Wang, Nano Lett. **1**, 443 (2001).

[10] K. E. Elkins, T. S. Vedantam, J. P. Liu, H. Zeng, S. Sun, Y. Ding, and Z. L. Wang, Nano Lett. **3**, 1647 (2003).

[11] F. Tournus, A. Tamion, N. Blanc, A. Hannour, L. Bardotti, B. Prevel, P. Ohresser, E. Bonet, T. Epicier, and V. Dupuis, Phys. Rev. B **77**, 144411 (2008).

[12] T. Miyazaki, O. Kitakami, S. Okamoto, Y. Shimada, Z. Akase, Y. Murakami, D. Shindo, Y. K. Takahashi, and K. Hono, Phys. Rev. B **72**, 144419 (2005).

[13] J. Penuelas, C. Andreazza-Vignolle, P. Andreazza, A. Ouerghi, and N. Bouet, Surf. Sci. **602**, 545 (2008).

[14] D. Alloyeau, C. Ricolleau, C. Mottet, T. Oikawa, C. Langlois, Y. Le Bouar, N. Braidy, and A. Loiseau, Nature Mater. **8**, 940 (2009).

[15] M. E. Gruner, G. Rollmann, P. Entel, and M. Farle, Phys. Rev. Lett. **100**, 087203 (2008).

[16] S. Stappert, B. Rellinghaus, M. Acet, and E. F. Wassermann, J. Cryst. Growth **252**, 440 (2003).

[17] R. M. Wang, O. Dmitrieva, M. Farle, G. Dumpich, H. Q. Ye, H. Poppa, R. Kilaas, and C. Kisielowski, Phys. Rev. Lett. **100**, 017205 (2008).

[18] F. Baletto, R. Ferrando, A. Fortunelli, F. Montalenti, and C. Mottet, J. Chem. Phys. **116**, 3856 (2002).

[19] J. Penuelas, P. Andreazza, C. Andreazza-Vignolle, H. C. N. Tolentino, M. De Santis, and C. Mottet, Phys. Rev. Lett. **100**, 115502 (2008).

[20] M. Müller and K. Albe, Phys. Rev. B **72**, 094203 (2005).

[21] C. Mottet, G. Treglia, and B. Legrand, Phys. Rev. B **66**, 045413 (2002).

[22] B. Abécassis, F. Testard, O. Spalla, and P. Barboux, Nano Lett. **7**, 1723 (2007).

[23] S. J. L. Billinge and I. Levin, Science **316**, 561 (2007).

[24] G. Renaud, R. Lazzari, and F. Leroy, Surf. Sci. Rep. **64**, 255 (2009).

[25] R. Baudoing-Savois, M. De Santis, M. C. Saint-Lager, P. Dolle, O. Geaymond, P. Taunier, P. Jeantet, J. P. Roux, G. Renaud, A. Barbier, O. Robach, O. Ulrich, A. Mougin, and G. Bérard, Nucl. Instrum. Methods Phys. Res. B **149**, 213 (1999).

[26] S. Ferrer and F. Comin, Rev. Sci. Instrum. **66**, 1674 (1995).

[27] C. Revenant, F. Leroy, G. Renaud, R. Lazzari, A. Letoublon, and T. Madey, Surf. Sci. **601**, 3431 (2007).

[28] R. Lazzari, J. Appl. Crystallogr. **35**, 406 (2002).

[29] J. Penuelas, P. Andreazza, C. Andreazza-Vignolle, C. Mottet, M. De Santis, and H. C. N. Tolentino, Eur. Phys. J. Spec. Top. **167**, 19 (2009).

[30] K. Koga, H. Takeo, T. Ikeda, and K. I. Ohshima, Phys. Rev. B **57**, 4053 (1998).

[31] D. Reinhard, B. D. Hall, D. Ugarte, and R. Monot, Phys. Rev. B **55**, 7868 (1997).

[32] J. M. Cowley, Phys. Rev. **120**, 1648 (1960).

[33] W. Grange, C. Ulhaq-Bouillet, M. Maret, and J. Thibault, Acta Mater. **49**, 1439 (2001).

[34] S. H. Whang, Q. Feng, and Y. O. Gao, Acta Mater. **46**, 6485 (1998).

[35] M. C. Fromen, P. Lecante, M. J. Casanove, P. B. Guillemaud, D. Zitoun, C. Amiens, B. Chaudret, M. Respaud, and R. E. Benfield, Phys. Rev. B **69**, 235416 (2004).

[36] C.-Yu Ruan, Y. Murooka, R. K. Raman, and R. A. Murdick, Nano Lett. **7**, 1290 (2007).

[37] V. Rosato, M. Guillopé, and B. Legrand, Philos. Mag. A **59**, 321 (1989).

[38] F. Cleri and V. Rosato, Phys. Rev. B **48**, 22 (1993).

[39] M. S. Daw and M. I. Baskes, Phys. Rev. B **29**, 6443 (1984).

[40] S. M. Foiles, M. I. Baskes, and M. S. Daw, Phys. Rev. B **33**, 7983 (1986).

[41] A. Dannenberg, M. E. Gruner, A. Hucht, and P. Entel, Phys. Rev. B **80**, 245438 (2009).

[42] W. R. Tyson and W. A. Miller, Surf. Sci. **62**, 267 (1977).

[43] R. Hultgren, P. D. Desai, D. T. Hawkins, M. Gleiser, and K. K. Kelley, *Values of the Thermodynamic Properties of Binary Alloys* (American Society for Metals, Metals Park, OH/Jossey-Bass, Berkley, 1981).

[44] L. Delfour, J. Creuze, and B. Legrand, Phys. Rev. Lett. **103**, 205701 (2009).

[45] S. Núñez and R. L. Johnston, J. Phys. Chem. C **114**, 13255 (2010).

[46] D. Bochicchio and R. Ferrando, Nano Lett. (to be published).

[47] G. Barcaro, R. Ferrando, A. Fortunelli, and G. Rossi, J. Phys. Chem. Lett. **1**, 111 (2010).

[48] F. Ducastelle, *Order and Phase Stability in Alloys* (North-Holland/Elsevier Science, Amsterdam, 1991).

[49] F. Ding, A. Rosén, and K. Bolton, Phys. Rev. **70**, 075416 (2004).

[50] H. Zhang and J. F. Banfield, Nano Lett. **4**, 713 (2004).

[51] H. Zhu and R. S. Averback, Philos. Mag. Lett. **73**, 27 (1996).